

Assessment of Sea-Level Rise Impacts on Salt-Wedge Intrusion in Idealized and Neretva River Estuary

Nino Krvavica^{a,*}, Igor Ružić^a

^a *University of Rijeka, Faculty of Civil Engineering, Radmile Matejcic 3, 51000 Rijeka, Croatia*

Abstract

Understanding the response of estuaries to sea-level rise is crucial in developing a suitable mitigation and climate change adaptation strategy. This study investigates the impacts of rising sea levels on salinity intrusion in salt-wedge estuaries. The sea-level rise impacts are assessed in idealized estuaries using simple expressions derived from a two-layer hydraulic theory, and in the Neretva River Estuary in Croatia using a two-layer time-dependent model. The assessment is based on three indicators - the salt-wedge intrusion length, the seawater volume, and the river inflows needed to restore the baseline intrusion. The potential SLR was found to increase all three considered indicators. Theoretical analysis in idealized estuaries suggests that shallower estuaries are more sensitive to SLR. Numerical results for the Neretva River Estuary showed that SLR may increase salt-wedge intrusion length, volume, and corrective river inflow. However, the results are highly non-linear because of the channel geometry, especially for lower river inflows. A theoretical assessment of channel bed slope impacts on limiting a potential intrusion is therefore additionally discussed. This findings emphasize the need to use several different indicators when assessing SLR impacts.

Keywords: climate change, sea level changes, salt-wedge estuaries, salinity stratification, two-layer models, saline intrusion

*Corresponding author

Email address: nino.krvavica@uniri.hr (Nino Krvavica)

1. Introduction

One of the most prominent consequences of ongoing climate change is the sea-level rise (SLR). The most recent report on changes in global and regional mean sea levels, sea-level extremes and waves is provided in the Fifth Assessment Report of the Intergovernmental Panel for Climate Change (IPCC) (Church et al., 2013). Although the effects that climate change will have in the future are uncertain, all recent studies agree that global sea levels will rise to some extent. A global SLR of 19 cm has been recorded over the period 1901-2010, with long-term projections suggesting that an increase with respect to 1986-2005 mean will lie within the range of 32-82 cm by the end of the twenty-first century (Church et al., 2013).

Sea-level rise has been recognized as a major threat to low-lying coastal environments, such as wetlands, salt marshes, and lagoons, with potentially devastating consequences (Kirwan et al., 2010; Cui et al., 2015; Carrasco et al., 2016; Sampath and Boski, 2016; Bigalbal et al., 2018). Estuaries are especially vulnerable coastal areas, because the seawater intrusion may endanger a fragile estuarine ecosystem and decrease the freshwater quality used for agricultural or water supply systems. Therefore, predicting and quantifying the salinity changes along estuaries is one of the key issues for water management in coastal areas.

In the past decade, numerous studies have investigated the impacts of rising sea levels in estuaries. Majority of these studies have found that SLR changes the water salinity in estuaries. In particular, increased seawater intrusion lengths and higher average salinities resulting from SLR have been predicted in the San Francisco Bay (Chua and Fringer, 2011; Chua and Xu, 2014), Delaware Estuary (Ross et al., 2015), Snohomish River Estuary (Yang et al., 2015), Chesapeake Bay (Hong and Shen, 2012) and its tributaries James and Chickahominy Rivers (Rice et al., 2012) in USA, Yangtze River Estuary (Li et al., 2015; Chen et al., 2016) and Nandu River Estuary (He et al., 2018) in China, Simjin River Estuary in Korea (Shaha et al., 2012), Wu River Estuary in Taiwan (Chen et al.,

2015), Gorai River network in Bangladesh (Bhuiyan and Dutta, 2012), Bahman-shir Estuary in the Persian Gulf (Etemad-Shahidi et al., 2015), Sebua Estuary in Morocco (Haddout and Maslouhi, 2018), Gironde Estuary in France (van Maanen and Sottolichio, 2018), as well as 96 estuaries in England and Wales (Prandle and Lane, 2015).

Tian (2019) examined several factor that control the seawater intrusion and found that the river flow rate is the dominant factor, followed by the sea level, which prevails in seasonal variations. Wind, on the other hand, has an impact only in shorter time scales. The channel geometry is also an important factor. Namely, the channel meanders can reduce stratification, change the two-layer circulation, and therefore alter the potential seawater intrusion (Tian, 2019). In addition to increasing seawater intrusion and average salinity, several recent studies have found that SLR may also strengthen stratification (Chua and Fringer, 2011), weaken vertical exchange (Hong and Shen, 2012), increase seawater volume (Hong and Shen, 2012), increase residence time and water age (Hong and Shen, 2012; Chen et al., 2015), and cause tidal amplifications (Kuang et al., 2014; van Maanen and Sottolichio, 2018).

Almost all studies mentioned above have focused on well-mixed or partially-mixed estuaries, which are characterized by homogeneous vertical column or weak stratification and gradual salinity changes along an estuary. On the other hand, studies investigating SLR impacts in salt-wedge estuaries, where freshwater and seawater layers are separated by a sharp interface (pycnocline), are less common. Strong vertical stratification, however, is found in many estuaries worldwide. Some prominent examples of salt-wedge estuaries are Mississippi and Merrimack Rivers in USA (Geyer and MacCready, 2014), Fraser River in Canada (MacDonald and Geyer, 2004), or the Ebro and Rhone Rivers in Europe (Ibañez et al., 1997). Strong stratification in estuaries is maintained by high river inflows, which dampen the vertical mixing caused by tidal motions (Geyer and MacCready, 2014). In micro-tidal conditions, stratification is usually persistent under all river inflows (Geyer and Ralston, 2011). In the Mediterranean region, for example, estuaries are strongly stratified even for relatively low river inflows

(Ibañez et al., 1997; Ljubenkov and Vranješ, 2012; Krvavica et al., 2016a,b). On the other hand, in tidally more dynamic environments, such as the Fraser Estuary, a strongly stratified structure may also be observed, but only during higher inflows (MacDonald and Geyer, 2004).

Although the dynamics of salt-wedge estuaries is well documented (Geyer and Ralston, 2011), there are hardly any studies available on the impact of SLR on the salt-wedge intrusion. This critical issue has been partially investigated in the Nile Estuary in Egypt (Mahgoub et al., 2014) and Rječina River Estuary in Croatia (Krvavica et al., 2016b). Both these studies showed that the tip of the salt-wedge may intrude further upstream under potential SLR. Recently, Tsz Yeung Leung et al. (2018) simulated the salt-wedge behaviour in the Fraser River Estuary in Canada under several climate and man-made changes. They also reported increased intrusion lengths, but additionally found that during low flow conditions, SLR may become more significant than changes in the river flow regime.

Considering that there are only a few comprehensive studies on SLR impacts on the salt-wedge intrusion, and almost no such studies in microtidal environments, the main aim of this study is to expand the knowledge on this topic. In contrast to previous studies that presented their findings for individual estuaries, this work is based on a more theoretical analysis of idealized estuaries, and numerical modelling of a salt-wedge estuary characteristic for microtidal environments. The theoretical analysis and simple analytical expressions are derived from a two-layer hydraulic theory, which is considered a satisfactory approximation in strongly stratified conditions. A wide range of idealized estuaries is considered here to provide a more general assessment of SLR impacts on seawater intrusion, and to remove the influence of channel geometry, in particular, bed elevations and width variations. The findings from theoretical analyses are substantiated by an example of a microtidal Neretva River Estuary in Croatia. Furthermore, along with the seawater intrusion length, as a common indicator for SLR impacts, we propose two additional indicators - the seawater volume and the river inflow increase needed to restore the baseline intrusion.

The proposed aims arise from two main hypothesis of this work: a) theoretical analysis derived from a two-layer hydraulic theory is an adequate tool for a generalized assessment of the SLR impacts on seawater intrusion in salt-wedge estuaries, and b) SLR impacts can be quantified by computing the changes in the salt-wedge intrusion length and volume, as well as the river inflow increase needed to restore the baseline intrusion.

2. Study area

2.0.1. Neretva River

Neretva River is the largest river in the eastern part of the Adriatic Basin. It is 215 km long, and for the most part, it flows through Bosnia and Herzegovina (BiH). For the final 22 km, it flows through Croatia before it enters the Adriatic Sea. Its catchment area is estimated to 10,240 km², of which only 280 km² is located in Croatia (Ljubenkovic and Vranješ, 2012; Oskoruš et al., 2019). Neretva River is a typical mountain river in its upper and middle part, but in the lower reaches, it forms a wide alluvial delta covering approximately 12,000 hectares (Fig. 1).

2.0.2. Neretva River Estuary

Lower reaches of the Neretva River are one of the most important and productive agricultural areas in Croatia. Unfortunately, the vicinity of the Adriatic Sea poses a threat to the future of the agricultural industry in this area. Namely, there are significant challenges with deteriorating freshwater quality for irrigation caused by the salinity intrusion, as well as persistent salinization of the groundwater and soil during summer months. These problems are expected to become even more severe in the future under climate change and a potential rise of sea levels, as well as the reduction of freshwater inflow during the summer.

The location and channel geometry of the Neretva River Estuary is shown in Fig. 1. Its mean channel depth is 8.5 m and the mean channel width is 132 m, both with some variations. The dynamics of the Neretva River Estuary is

governed by tidal oscillations of the Adriatic Sea and upstream inflows, which depend on the operational aspects and management of the hydro-power system of accumulations and dams built in its middle reaches located in BiH. Neretva River has a pronounced seasonal character, typical for Mediterranean climate, with a well defined high flow season from October to April, and a low flow period from May to September. During the summer, when irrigation needs are more pronounced, the precipitation and river inflows are at their lowest, and the seawater regularly intrudes over 20 km upstream (Ljubenković and Vranješ, 2012).

Although water levels in its lower part have been measured since 1957, a systematic flow rate and conductivity measurements were established only in 2015. Short-term data at the station Metković indicates that its mean annual flow rate is $325 \text{ m}^3/\text{s}$, while a maximum measured flow rate is $1375 \text{ m}^3/\text{s}$ (Oskoruš et al., 2019). Minimum flow rate is regulated by an international agreement between Croatia and BiH, which states that a minimum $50 \text{ m}^3/\text{s}$ must be released from the hydro-power plant Mostar (Oskoruš et al., 2019).

2.0.3. Tides and sea levels in the Adriatic Sea

The tides in the Adriatic Sea are of a mixed type with relatively low amplitudes. The maximum astronomical tidal amplitude recorded between 1953 and 2006 at the Bakar tidal gauging station was 123 cm; however, mean tidal amplitudes do not exceed 30 cm (Rezo and Pavasović, 2014). Highest recorded sea level at the Neretva River mouth (in period 1977-2018) was 120 cm a.s.l., and the lowest -25 cm a.s.l. (Oskoruš et al., 2019).

Because of the microtidal environment and high freshwater flow rates, the Neretva River Estuary is a typical salt-wedge estuary according to classification by Geyer and MacCready (2014), occupying the upper-left corner of the estuarine parameter space with freshwater Froude number higher than 0.1 and mixing number under 0.4. Salinity profile measurements conducted by Ljubenković and Vranješ (2012) shown very strong stratification with pycnocline thickness always under 0.5 m. Similar salinity profiles in the Rječina River (also located on

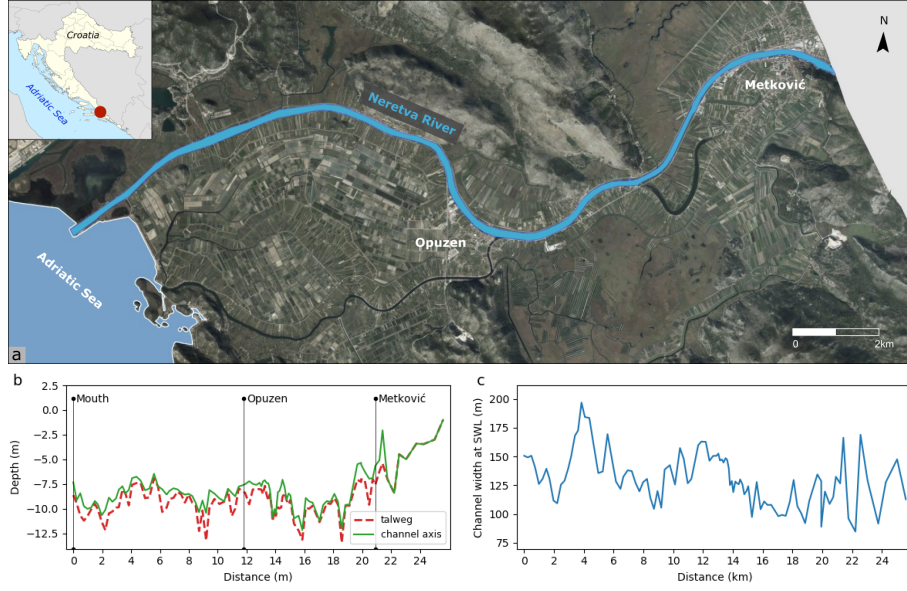


Figure 1: Neretva River Estuary: a) geographical location and digital ortophoto, b) longitudinal bottom profile and c) channel width variations at SWL (± 0 m a.s.l.)

the eastern Adriatic coast) indicated buoyancy frequencies well over $N^2 > 0.1$ (Krvavica et al., 2016b). Geyer et al. (2008) reported typical values for N^2 ranging from 0.0025 to 0.01 s^{-2} for partially mixed estuaries and up to 0.1 s^{-2} for salt-wedge estuaries. In this case, the stratification is so pronounced that it even exceeds the upper values usually associated with salt-wedge estuaries. Such a strong stratification is a result of extremely low tidal dynamics of the Adriatic Sea.

A comprehensive overview of the literature on the sea-level research in the Adriatic Sea is given by Vilibić et al. (2017). The Mediterranean Sea, and the Adriatic Sea as its integral part, has been recognized as one of the most sensitive to climate change. Some projections for the period between 1990-2000 and 2040-2050 show up to 25.6 cm increase averaged over the Mediterranean (and Adriatic) Sea. Projections for the basin-averaged steric SLR in the Adriatic Sea over the twenty-first century point to only 13 cm. However, when the contribution of salinity and temperature are taken into account to assess both mass

and steric components on a local scale, a sea-level rise of 49.7 cm is expected for the period 2000-2100. For a more detailed explanation of the salinity and temperature contribution to SLR in the Mediterranean basin see the study by Jordà and Gomis (2013). This is close to findings by Tsimplis et al. (2012), who used tidal gauge records from almost all stations in the Adriatic Sea to analyse trends in sea levels and estimated an increase in the range from 2.0 ± 0.9 to 3.4 ± 1.1 mm/year, which suggests that SLR by the year 2100 could reach up to 45 cm. More recent analysis, however, suggests that the sea-level rise is rapidly increasing (Church et al., 2013), and that trends derived from past and present measurements underestimate potential SLR in the future. Therefore, we considered a more extreme scenario in the Adriatic Sea with sea levels rising to 100 cm with respect to present conditions.

3. Materials and Methods

3.1. *Hydraulics of Salt-Wedge Estuaries*

Although three-dimensional (3D) hydrodynamic models are regularly used for computing physical process in estuaries (Mohammed and Scholz, 2017), salt-wedge estuaries are adequately represented by a simpler two-layer hydraulic theory (Sargent and Jirka, 1987; Krvavica et al., 2016b, 2017). Two-layer theory is derived from coupled shallow water equations (SWE) - we assume that the vertical structure can be represented by two shallow layers of different densities separated by a pycnocline of zero thickness (see Fig. 2). Furthermore, we assume, under the usual SWE theory, that the velocity and density are uniform over each layer, vertical accelerations are negligible, the pressure is hydrostatic, the channel bed slope is mild, and the viscous effects such as friction and turbulence are represented by simple empirical equations. Also, we assume that the flow is predominately one-dimensional (1D) and that the channel is prismatic with rectangular cross section of uniform width.

Schijf and Schönflöd (1953) and Stommel and Farmer (1953) were among first to develop a mathematical theory for two-layer flows. Recently, Geyer

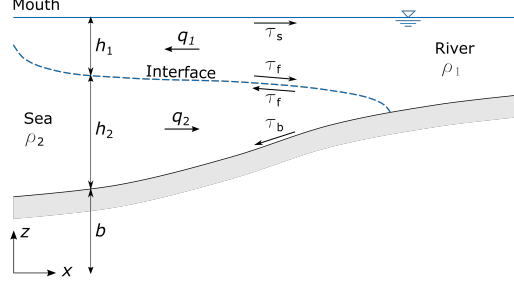


Figure 2: Characteristic longitudinal section of a salt-wedge estuary

and Ralston (2011) provided a good insight into the current knowledge on the dynamics of strongly stratified estuaries. The governing system of partial differential equations (PDEs) for a one-dimensional two-layer shallow water flow in prismatic channels with constant width (Fig. 2) is written as a coupled system of continuity and momentum equations (Schijf and Schönfeld, 1953):

$$\frac{\partial h_1}{\partial t} + \frac{\partial q_1}{\partial x} = 0 \quad (1)$$

$$\frac{\partial q_1}{\partial t} + \frac{\partial}{\partial x} \left(\frac{q_1^2}{h_1} + \frac{g}{2} h_1^2 \right) = -g h_1 \frac{db}{dx} - g h_1 \frac{\partial h_2}{\partial x} - \frac{\tau_f}{\rho_1} \quad (2)$$

$$\frac{\partial h_2}{\partial t} + \frac{\partial q_2}{\partial x} = 0 \quad (3)$$

$$\frac{\partial q_2}{\partial t} + \frac{\partial}{\partial x} \left(\frac{q_2^2}{h_2} + \frac{g}{2} h_2^2 \right) = -g h_2 \frac{db}{dx} - g h_2 \frac{\rho_1}{\rho_2} \frac{\partial h_1}{\partial x} + \frac{\tau_f - \tau_b}{\rho_2} \quad (4)$$

where x is the coordinate along the channel axis, t is time, $h_i(x, t)$ is the thickness of i -th layer, $b(x)$ is the channel bottom function, $q_i(x, t)$ is the layer flow rate per unit width, ρ_i is the layer density, g is acceleration of gravity, τ_f is the interfacial shear stress, τ_b is the shear stress between channel bed and lower layer fluid, and subscript $i = 1, 2$ denotes the upper and lower layer, respectively. The shear stresses may be parametrized using a quadratic drag equation:

$$\tau_f = C_f \rho_1 |u_1 - u_2| (u_1 - u_2) \quad (5)$$

and

$$\tau_b = C_w \rho_2 |u_2| u_2 \quad (6)$$

where C_f is the interfacial friction factor, C_b is the bed friction factor and $u_i(x, t) = q_i(x, t)/h_i(x, t)$ is the layer velocity.

At constant sea-water level (SWL) and river inflow q , an equilibrium is established between the buoyancy pressure gradients, friction forces, and inertial forces, and eventually a steady-state flow forms (Sargent and Jirka, 1987). This two-layer stationary form is sometime called an arrested salt-wedge, which is characterized by a stagnant lower layer called a salt-wedge because of its shape, and an upper layer of constant flow rate.

A mathematical model for an arrested salt-wedge is derived from Eqs. (1)-(4) following Schijf and Schönfeld (1953). Time derivatives are neglected, negative flow is asserted in the upper layer $q_1 = q < 0$ (because x increases in the upstream direction) and zero-flow in the lower layer $q_2 = 0$. Momentum equations are then subtracted from each other under the rigid lid approximation, and a single ordinary differential equation (ODE) is obtained that describes the pycnocline depth along the channel axis:

$$\frac{dh_1}{dx} = \frac{F_d^2}{1 - F_d^2} C_f \left(1 + r \frac{h_1}{h_2} \right). \quad (7)$$

where $r = \rho_1/\rho_2$ is the density ratio and F_d is the internal Froude number for the upper layer:

$$F_d = \frac{q_1}{\sqrt{g(1-r)h_1^3}}. \quad (8)$$

Note that Eq. (7) corresponds to the one derived by Geyer and Ralston (2011) or Krvavica et al. (2014) in a slightly different form. This equation defines how the upper layer changes along the estuary, but it is not valid upstream from the tip of the salt-wedge. Also, it is clear that the solution is singular when the internal Froude number is equal to one $F_d = 1$. This may occur at the hydraulic control, which is usually located at the river mouth, where the numerical integration should begin (Geyer and Ralston, 2011). Note that the hydraulic control may also be present at other locations along channels, if there are strong lateral constrictions or abrupt bed elevations (Poggioli and Horner-Devine, 2015).

For idealized estuaries, Eq. (7) may be further simplified by considering a horizontal channel bed ($b(x) = \text{const.}$) and introducing the following non-dimensional parameters:

$$\varphi = h_1/H_0, \quad \chi = C_f x/H_0, \quad (9)$$

where H_0 is a constant total depth in a prismatic channel with no bed elevations. Also, the internal Froude number for the river (Geyer and Ralston, 2011) is

$$F_0 = F(q, H_0, r) = \frac{q}{\sqrt{g(1-r)H_0^3}} = F_d \varphi^{3/2}. \quad (10)$$

Note, that F_0 is the same as F_d when the upper layer flow rate q_1 equals river inflow q (which is always true for idealized arrested salt-wedges) and thickness h_1 equals total depth H_0 (which is true for idealized channels upstream from the tip of the salt-wedge). Furthermore, this non-dimensional parameter corresponds to the net barotropic flow U_0 introduced by Armi and Farmer (1986) as the key dynamical parameter governing a two-layer hydraulic flow.

Substituting the parameters defined by Eqs. (9) and (10), and using the Boussinesq approximation, which neglects the density ratio r everywhere except where multiplied by g (Tritton, 1988), Eq. (7) becomes

$$\frac{d\varphi}{d\chi} = \frac{F_0^2}{\varphi^3 - F_0^2} \left(\frac{1}{1 - \varphi} \right). \quad (11)$$

Equation (11) is then integrated over non-dimensional depth to obtain an integral form of the equation:

$$\chi = \int_{\varphi_1}^{\varphi_2} \left[\frac{F_0^2}{\varphi^3 - F_0^2} \left(\frac{1}{1 - \varphi} \right) \right]^{-1} d\varphi. \quad (12)$$

To find the salt-wedge length, Eq. (12) is integrated between the hydraulic control (usually located at the river mouth) and the tip of the salt-wedge. These boundaries are introduced as the lower and upper integral limits. Considering that $F_d = 1$ is true at the hydraulic control point, we can combine Eq. (8) and Eq. (10) to obtain non-dimensional upper and lower layer depths at the river mouth (critical depths):

$$\varphi_{cr} = h_{1,cr}/H_0 = F_0^{2/3} \quad (13)$$

and

$$1 - \varphi_{cr} = h_{2,cr}/H_0 = 1 - F_0^{2/3}. \quad (14)$$

Similarly, at the salt-wedge tip we have $h_1 = H_0$, therefore $\varphi_2 = 1$.

Integrating Eq. (12) between $\varphi_1 = F_0^{2/3}$ and $\varphi_2 = 1$ leads to the following analytical expression for a non-dimensional length L^* of the salt-wedge intrusion:

$$L^*(F_0) = \frac{1}{20} \left(15F_0^{2/3} - 6F_0^{4/3} - 10 + F_0^{-2} \right). \quad (15)$$

A dimensional salt-wedge length L can then be restored from Eq. (9) by computing $L = H_0 L^*/C_f$, and then we obtain a well-known analytical expression derived by Schijf and Schönflöd (1953):

$$L(H_0, C_f, F_0) = \frac{H_0}{20C_f} \left(15F_0^{2/3} - 6F_0^{4/3} - 10 + F_0^{-2} \right). \quad (16)$$

It is clear that the intrusion length is a function of the channel depth H_0 , interfacial friction factor C_f and internal Froude number F_0 (defined upstream from the salt-wedge).

The shape of the salt-wedge may be computed similarly, but in a discrete form by repeatedly integrating Eq. (12), for a series of boundary values starting from $\varphi_1 = F_0^{2/3}$ and $\varphi_2 = \varphi_1 + \Delta\varphi$, where $\Delta\varphi$ is a spatial step. We increase $\Delta\varphi$ until we reach $\varphi_2 = 1$. In this way, each φ_2 is the non-dimensional upper layer thickness at a computed non-dimensional distance χ from the hydraulic control point. Discrete function $\varphi(\chi)$, therefore, gives a non-dimensional function for the thickness of the salt-wedge, i.e. pycnocline depth.

We see that arrested salt-wedges are fully defined by three components - initial pycnocline depth, i.e. critical lower layer depth $h_{2,cr}$ or $1 - \varphi_{cr}$, length L or L^* , and pycnocline function, i.e., thickness depth variability from the salt-wedge tip to the hydraulic control point defined by set of points (h_2, x) or $(1 - \varphi_2, \chi)$ in a non-dimensional form.

Combining these parameters, we can derive an additional one - salt-wedge volume per unit width V , defined as the total volume of seawater below the pycnocline, which is obtained by integrating $h_2(x)$ from the river mouth ($x = 0$)

to the salt-wedge tip ($x = L$):

$$V(L, h_2) = \int_0^L h_2(x) dx, \quad (17)$$

or in a non-dimensional form:

$$V^*(L, \varphi) = \frac{V}{LH_0} = \frac{1}{L} \int_0^L (1 - \varphi) dx. \quad (18)$$

Note that value V^* represents the total seawater to fresh-water ratio along the salt-wedge. This information may sometimes be more important than the intrusion length as it directly relates to salinity intrusion into aquifer, especially in highly permeable mediums (Shalem et al., 2019).

These non-dimensional salt-wedge parameters are presented in Figure 3 in relation to internal Froude numbers. Non-dimensional friction length is shown in Fig. 3a, critical lower layer depth in Fig. 3b, salt-wedge interface in Fig. 3c and seawater volume in Fig. 3d. Two-layer hydraulic theory predicts that larger values of F_0 correspond to shorter salt-wedge intrusion lengths, thinner seawater layers, and lower volumes of seawater in estuaries. The shape of the pycnocline is less sensitive to F_0 .

Considering that the internal Froude number is a function of the river inflow and estuary depth, it also follows that salt-wedge intrusion length, thickness and volume increase with the estuary depth and decrease with the river inflow, which has been confirmed by field measurements in microtidal estuaries (Krvavica et al., 2016a,b). Since SLR directly increases the estuary depth, it should also increase the salt-wedge intrusion length and volume. Note, that the salt-wedge intrusion in a single estuary may shift tens of kilometres upstream or downstream depending on river inflows and sea levels (Geyer and Ralston, 2011).

3.2. *Hydrodynamic model for two-layer flow in salt-wedge estuaries with irregular geometry*

3.2.1. *Governing equations*

A numerical model STREAM-1D (STRatified EstuArine Model) (Krvavica et al., 2016b, 2017) is similarly based on one-dimensional time-dependent two-

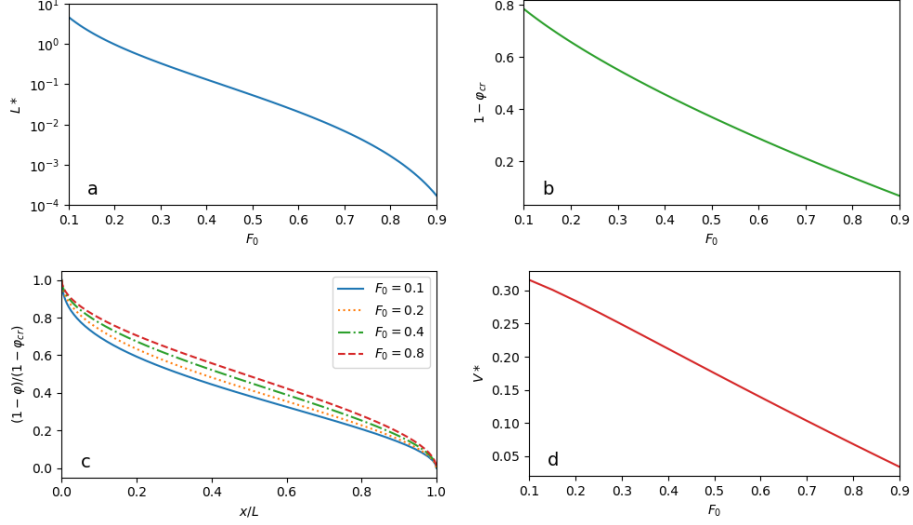


Figure 3: Salt-wedge parameters given as a function of internal Froude numbers: a) non-dimensional salt-wedge length, b) non-dimensional thickness of the salt-wedge at the hydraulic control, c) non-dimensional interface function, d) non-dimensional salt-wedge volume.

layer shallow water equations. It shares the simplifications and assumptions with the two-layer theory defined by Eqs. (1)-(4). The governing equations, however, are extended to account for irregular channel geometry, as well as a full shear stress and entrainment parametrization. Therefore, STREAM-1D may be used to simulate the dynamics of salt-wedges in channelized estuaries under different combinations of sea levels and river flows rates.

The governing equations are written as the following coupled system of conservation laws with source terms (Krvavica et al., 2016b):

$$\frac{\partial \mathbf{w}}{\partial t} + \frac{\mathbf{f}(\boldsymbol{\sigma}, \mathbf{w})}{\partial x} = \mathbf{B}(\boldsymbol{\sigma}, \mathbf{w}) \frac{\partial \mathbf{w}}{\partial x} + \mathbf{v}(\boldsymbol{\sigma}, \mathbf{w}) + \mathbf{g}(\boldsymbol{\sigma}, \mathbf{w}) + \mathbf{s}(\boldsymbol{\sigma}, \mathbf{w}), \quad (19)$$

where \mathbf{w} is the vector of conserved variables:

$$\mathbf{w} = \left\{ A_1 \quad Q_1 \quad A_2 \quad Q_2 \right\}^T, \quad (20)$$

vector $\mathbf{f}(\boldsymbol{\sigma}, \mathbf{w})$ is the flux:

$$\mathbf{f}(\boldsymbol{\sigma}, \mathbf{w}) = \left\{ Q_1 \quad \frac{Q_1^2}{A_1} + \frac{g}{2\sigma_1} A_1^2 \quad Q_2 \quad \frac{Q_2^2}{A_2} + \frac{g}{2\sigma_2} A_2^2 \right\}^T, \quad (21)$$

and term $\mathbf{B}(\boldsymbol{\sigma}, \mathbf{w}) \frac{\partial \mathbf{w}}{\partial x}$ appears as a result of coupling the two-layer system, where matrix $\mathbf{B}(\boldsymbol{\sigma}, \mathbf{w})$ is defined as

$$\mathbf{B}(\boldsymbol{\sigma}, \mathbf{w}) = \begin{bmatrix} 0 & 0 & 0 & 0 \\ 0 & 0 & -g \frac{A_1}{\sigma_1} & 0 \\ 0 & 0 & 0 & 0 \\ -gr \frac{A_2}{\sigma_1} & 0 & 0 & 0 \end{bmatrix}. \quad (22)$$

where A_i is the layer cross section area, Q_i is the layer flow rate, and $\boldsymbol{\sigma} = \{\sigma_1 \ \sigma_2 \ \sigma_3\}^T$ is the vector of channel widths.

The additional source terms have been split into three parts; the first vector $\mathbf{v}(\boldsymbol{\sigma}, \mathbf{w})$ corresponds to derivatives of $\boldsymbol{\sigma}$:

$$\mathbf{v}(\boldsymbol{\sigma}, \mathbf{w}) = \left\{ 0 \quad \frac{g}{2} \frac{\partial}{\partial x} \left(\frac{1}{\sigma_1} \right) A_1^2 \quad 0 \quad \frac{g}{2} \frac{\partial}{\partial x} \left(\frac{1}{\sigma_2} \right) A_2^2 \right\}^T, \quad (23)$$

the second vector $\mathbf{g}(\boldsymbol{\sigma}, \mathbf{w})$ corresponds to the channel bed, width, and wetted cross-section area (*i.e.*, irregular geometry):

$$\mathbf{g}(\boldsymbol{\sigma}, \mathbf{w}) = \left\{ \begin{array}{c} 0 \\ gA_1 \left[\frac{1}{\sigma_1} \frac{\partial}{\partial x} (A_1 + A_2) - \frac{\partial}{\partial x} (b + h_2 + h_1) \right] \\ 0 \\ gA_2 \left[\frac{1}{\sigma_2} \frac{\partial A_2}{\partial x} + \frac{r}{\sigma_1} \frac{\partial A_1}{\partial x} - \frac{\partial}{\partial x} (b + h_2 + rh_1) \right] \end{array} \right\}. \quad (24)$$

and the third vector $\mathbf{s}(\boldsymbol{\sigma}, \mathbf{w})$ corresponds to the friction and entrainment:

$$\mathbf{s}(\boldsymbol{\sigma}, \mathbf{w}) = \mathbf{s}_F(\boldsymbol{\sigma}, \mathbf{w}) + \mathbf{s}_E(\boldsymbol{\sigma}, \mathbf{w}), \quad (25)$$

$$\mathbf{s}_F(\boldsymbol{\sigma}, \mathbf{w}) = \left\{ \begin{array}{c} 0 \\ \frac{\tau_w}{\rho_1} P_1 + \frac{\tau_i}{\rho_1} \sigma_3 \\ 0 \\ \frac{\tau_b}{\rho_2} P_2 - \frac{\tau_i}{\rho_2} \sigma_3 \end{array} \right\}, \quad \mathbf{s}_E(\boldsymbol{\sigma}, \mathbf{w}) = \left\{ \begin{array}{c} \frac{1}{r} w_e \sigma_3 \\ \frac{Q_1}{A_1} w_e \sigma_3 \\ -w_e \sigma_3 \\ -\frac{Q_2}{A_2} w_e \sigma_3 \end{array} \right\}, \quad (26)$$

where τ_w is shear stress between upper layer fluid and channel walls, τ_i is the shear stress at the interface between the layers, τ_b is the shear stress between the lower layer fluid and channel bed, and w_e is the entrainment velocity.

3.2.2. Numerical scheme

The numerical scheme used to solve the governing equations is based on the finite volume method, specifically, the efficient semi-analytical Roe scheme (Krvavica et al., 2018). The scheme is explicit in time and stable under the usual CFL condition. It is well balanced, shock-capturing, and considered to be the most accurate first-order scheme. STREAM-1D has been thoroughly tested and validated for other salt-wedge estuaries (Krvavica et al., 2016b, 2017).

4. Results

The results section consists of two parts. First, we theoretically assess the impacts of SLR on the seawater intrusion in idealized estuaries, and then, we demonstrate the impacts of potential SLR in the Neretva River Estuary in Croatia to validate and illustrate some limitations of theoretical analysis. Furthermore, this practical example is presented to emphasize the importance of a more comprehensive assessment of SLR impacts in salt-wedge estuaries.

As defined previously, the impacts of SLR on salt-wedge intrusion in ideal estuaries and the Neretva River Estuary are assessed by considering three indicators:

- the salt-wedge intrusion length L ,
- the salt-wedge volume V ,
- the corrective river inflow needed to restore the baseline condition q_{corr} .

The salt-wedge intrusion length is a standard indicator for assessing the impacts of SLR. The salt-wedge volume reflects both the salt-wedge intrusion length and an overall increase of the pycnocline depth. The third indicator is introduced from the viewpoint of managing or mitigating the negative effects of SLR by increasing the river inflow to ensure that sufficient freshwater is available to restore the baseline intrusion length and ensure that sufficient freshwater is available for irrigation or water supply needs. This measure, however, is possible

only if some man-made system, such as a hydro-power plant or accumulation, is built upstream from the estuary.

4.1. Sea-level rise impacts in idealized estuaries

Sea-level rise in idealized estuaries is accounted for by considering a range of estuary depth increases:

$$H_{slr} = H_0 + \Delta H, \quad (27)$$

where ΔH denotes the water level increase resulting from SLR. To illustrate general SLR impacts, we considered values ranging from $\Delta H = 0$ cm (baseline) to $\Delta H = +100$ cm (maximum rise), and estuary channel depths ranging from 3 m to 15 m (which represents the majority of salt-wedge estuaries around the world). Internal Froude number are constrained between $0.1 < F_0 < 0.9$. Note that when F_0 approaches one, the flow becomes critical and the salt-wedge is completely pushed out from an estuarine channel. On the other hand, when F_0 approaches zero, the intrusion length goes to infinity and an estuary becomes completely occupied by the seawater.

SLR impacts on salt-wedge intrusion lengths are estimated by computing salt-wedge lengths from Eq. (16) for a given sea-level rise $L_{slr} = L(H_{slr}, F_{slr})$ and then comparing them to baseline lengths $L_0 = L(H_0, F_0)$, where the internal Froude number affected by SLR is given by $F_{slr} = F(q, H_{slr}, r)$ and baseline internal Froude number by $F_0 = F(q, H_0, r)$. Similarly, SLR impacts on the salt-wedge volume are estimated by computing the volume of seawater below the pycnocline from Eq. (17) for a given sea-level rise $V_{slr} = V(L_{slr}, h_{2,slr})$ and comparing them to baseline volumes $V_0 = V(L_0, h_2)$. Furthermore, if we denote the baseline river inflow by q , and the corrective river inflow (needed to restore the baseline salt-wedge intrusion) by q_{corr} , then it is easy to solve the following equation for q_{corr} :

$$L(H_0, F(q, H_0, r)) - L(H_{slr}, F(q_{corr}, H_{slr}, r)) = 0. \quad (28)$$

To quantify absolute values in addition to relative increases, we assumed relative

density $r = 0.97$ and interfacial friction factor $C_f = 5 \times 10^{-4}$, which is a gross estimate suggested by Geyer and Ralston (2011).

4.1.1. Assessing sea-level rise impacts by the salt-wedge length

Theoretical equation (16) for the salt-wedge length indicates that SLR increases the salt-wedge intrusion length from L_0 to L_{slr} by reducing the internal Froude number from F_0 to F_{slr} and increasing the total estuary depth from H_0 to H_{slr} . Note that SLR affects each estuary differently, the same absolute increase of SLR results in different relative changes of internal Froude number and channel depth. In other words, the magnitude of potential SLR impacts will depend on the estuary depth and river inflow.

Figs. 4a-c shows theoretical increases of salt-wedge intrusion lengths under rising sea-levels, for a predefined range of estuary depths and a low internal Froude number $F_0 = 0.2$. Similar relative values are obtained for other internal Froude numbers, but, obviously, absolute values vary according to results previously shown in Fig. 3. As expected, SLR increases the salt-wedge intrusion length under all conditions (Fig. 4a). The results show that shallower estuaries are more affected by SLR - salt-wedge intrusion lengths increase more in shallow estuaries for the same SLR (Figs. 4b, c). A recent study on a large sample of UK estuaries also reported that SLR impacts are more pronounced in shallower (< 10 m) and micro-tidal estuaries (Prandle and Lane, 2015).

4.1.2. Assessing sea-level rise impacts by the salt-wedge volume

In addition to increasing the salt-wedge intrusion length, SLR also rises the average pycnocline depth and consequently the total thickness of the salt-wedge. This dual increase is expressed by the salt-wedge volume defined by Eq. (17).

Figs. 4d-f shows theoretical increases of salt-wedge volumes under rising sea-levels, for a predefined range of estuary depths and a low internal Froude number $F_0 = 0.2$. Same as for the intrusion length, SLR increases the salt-wedge volume under all conditions (Fig. 4d). The results also suggest that shallower estuaries are more affected by SLR. Although absolute increases of the salt-wedge volume

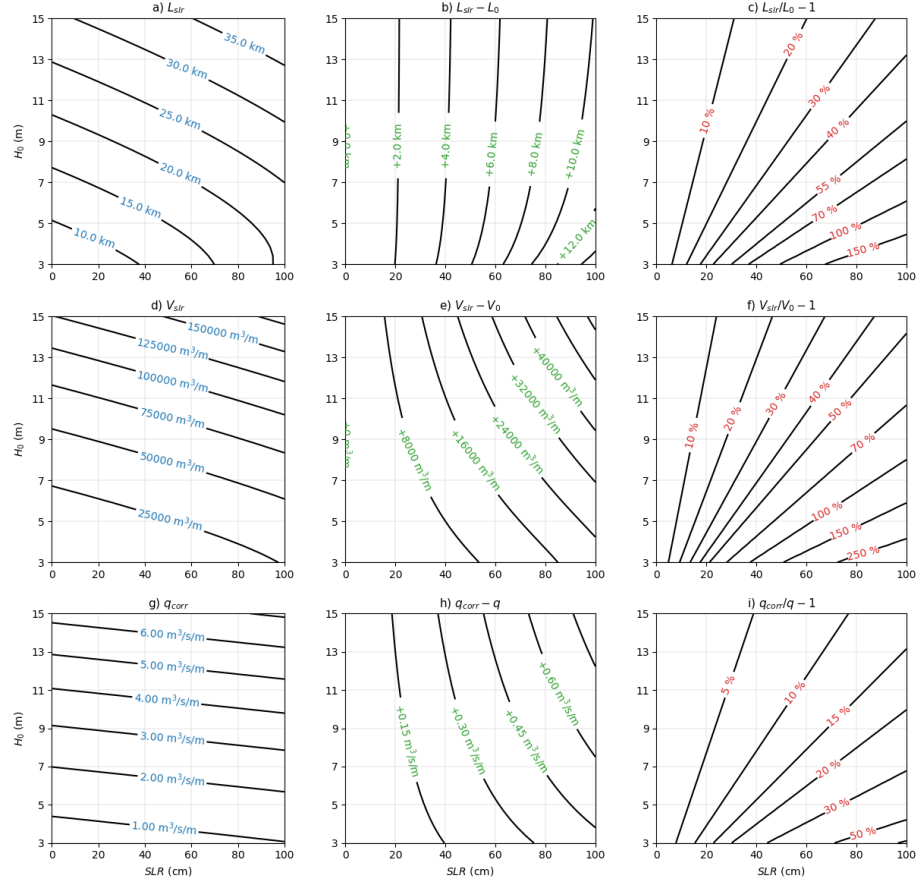


Figure 4: Theoretical impact of SLR on salt-wedge intrusion for $F_0 = 0.2$, with $r = 0.97$ and $C_f = 5 \times 10^{-4}$: a) total intrusion length, b) absolute length increase, c) relative length increase, d) total salt-wedge volume, e) absolute volume increase, f) relative volume increase, g) total corrective river inflow, h) absolute inflow increase, i) relative inflow increase

are larger in deeper estuaries, the relative increases are much higher in shallower estuaries for the same SLR (Fig. 4f).

4.1.3. Assessing sea-level rise impacts by the corrective river inflow

The corrective river inflow defines an additional flow rate needed to push out the salt-wedge to its baseline position. By increasing the river inflow, we increase the internal Froude number. Eq. (16), however, shows that it is not enough to just restore F_0 from F_{slr} , but the internal Froude number must be larger than F_0 to compensate for higher H_{slr} .

Figs. 4g-i shows theoretical increases of the corrective river inflow under rising sea-levels, for a predefined range of estuary depths and a low internal Froude number $F_0 = 0.2$. We see that for all conditions, the corrective river inflow needs to increase to balance longer salt-wedge intrusion (Fig. 4g). The results again suggest that shallower estuaries are more affected by SLR. Similarly as for the salt-wedge volumes, absolute increases are larger in deeper estuaries, but the relative increases are much higher in shallow estuaries for the same SLR (Fig. 4i).

4.2. Sea-level rise impacts in the Neretva River Estuary

4.2.1. Numerical model validation

Two-layer shallow water models have been previously applied and validated for the Neretva River Estuary (Ljubenkovic and Vranješ, 2012) and several other microtidal estuaries (Ljubenkovic, 2015; Krvavica et al., 2016b). The numerical results in the Neretva River Estuary showed a good agreement with salinity measurements throughout the year, under a wide range of hydrological conditions (Ljubenkovic and Vranješ, 2012). Furthermore, the STREAM-1D model was thoroughly tested and validated in the Rječina River estuary, which is also located on the Adriatic coast and exposed to identical tidal conditions (Krvavica et al., 2016b, 2017). Additionally, field measurements at several river estuaries on the Adriatic coast (Krvavica et al., 2016a; Ljubenkovic and Vranješ, 2012; Ljubenkovic, 2015), showed that a strong stratification is persistent throughout

the year because of microtidal conditions and that the two-layer theory is a reasonable approximation.

In this study, we validated the model after calibrating the channel bed roughness and interfacial friction factor in the Neretva River Estuary and comparing intrusion lengths, as well as upstream water levels to measurements. The validation is based on measurements from 2018 at the river mouth and upstream hydrological station Metković located 20.9 km from the river mouth (Fig. 1b).

First, we analysed the river inflow and compared the computed salt-wedge length to the measurements of the conductivity at the channel bottom at station Metković. These measurements show that the salt-wedge tip is located downstream from the Metković station for $Q > 180 \text{ m}^3/\text{s}$. Using this constraint, we calibrated the interfacial friction factor and found a good agreement with the measurements for $C_f = 6 \times 10^{-4}$. Note, that C_f may slightly vary along the salt-wedge and in time since its magnitude is some function of internal Reynolds and Froude (or bulk Richardson) number (Krvavica et al., 2017). However, for steady flow rates, and mild changes in the channel geometry, it can be considered constant. Similar friction factors were found in other salt-wedge estuaries (Geyer and Ralston, 2011; Ljubenkov and Vranješ, 2012; Krvavica et al., 2016a).

We also compared the numerical results to measured water levels at station Metković, and found the best agreement for Manning’s bed roughness coefficient $n = 0.03 \text{ s/m}^{1/3}$. The comparison of computed and measured water levels at station Metković for the entire 2018, indicated a root mean square error $RMSE = 12 \text{ cm}$, and Pearsons correlation coefficient $R = 0.96$.

4.2.2. Assessing SLR impacts on salt-wedge intrusion in the Neretva estuary

Parameters used for numerical simulations are given by the density ratio $r = 0.975$, interfacial friction factor $C_f = 6 \times 10^{-4}$, and Manning’s bed roughness coefficient $n = 0.03 \text{ s/m}^{1/3}$. Spatial step was $\Delta x = 10 \text{ m}$, and a variable time step was computed based on the stability condition $CFL = 0.8$. The simulation was performed until steady-state conditions were obtained.

First, we performed a series of simulations for three SLR cases, namely 0.0,

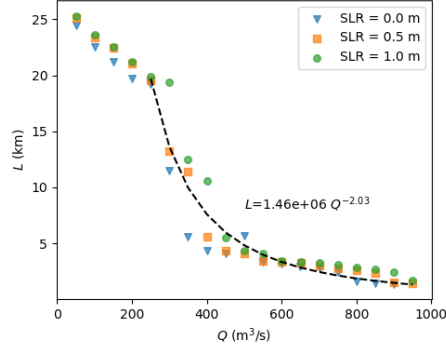


Figure 5: Salt-wedge intrusion lengths for a range of river inflows and three different sea-level rises ($R^2 = 0.91$)

0.5 and 1.0 m, and river inflows ranging from 50 to 1000 m^3/s , which roughly correspond to the range $F_0 = 0.15 - 0.75$. For each combination of SLR and Q we computed the salt-wedge intrusion length in the Neretva River Estuary.

Cumulative results shown in Fig. 5 indicate that the intrusion length may be related to the river inflow by the following power law (with $R^2 = 0.91$):

$$L = 1.46 \times 10^6 \times Q^{-2.03}. \quad (29)$$

Note that the exponent -2.03 is valid for all SLR, but only for higher river inflows, namely $Q > 250 \text{ m}^3/\text{s}$. At lower river inflows, the channel geometry (steeper channel bed slope) prevents longer intrusion lengths (see Fig. 1b). Such exponent agrees with a theoretical range of -2.0 to -2.5 found by Geyer and Ralston (2011) and confirms the importance of the river inflow in stratified estuaries in comparison to partially or well-mixed estuaries, where the exponent is one order of magnitude lower (Monismith et al., 2002). Even in some other salt-wedge estuaries, the exponent is usually lower, e.g. -0.19 in the Merrimack River Estuary (Ralston et al., 2010).

Quantifying the SLR impacts on the intrusion in the Neretva River Estuary is not so trivial. It seems that uneven channel bed plays an important part in the advancement of the salt-wedge when sea level increases. However, some trends are noticeable (Fig. 5). Evidently, SLR increases the salt-wedge intrusion length

under all hydrological conditions. The strongest impact of SLR on the intrusion length is observed for river inflows in the range $250 < Q < 500 \text{ m}^3/\text{s}$, when SLR may increase the intrusion length by 6 to 8 km further upstream (Fig. 5). As stated earlier, for $Q < 250 \text{ m}^3/\text{s}$, the expected salt-wedge length increase is prevented by the channel bed elevations, and for $Q > 500 \text{ m}^3/\text{s}$ the baseline salt-wedge length is much shorter, so that SLR has a lower overall impact – intrusions are increased by up to 2 km.

For a more detailed analysis of the SLR impacts in the Neretva River Estuary, we consider two hydrological scenarios: Case A defined by the river inflow $Q = 300 \text{ m}^3/\text{s}$ which corresponds to $F_d = 0.23$ at the salt-wedge tip, and Case B defined by the river inflow $Q = 50 \text{ m}^3/\text{s}$ which corresponds to $F_d = 0.16$ at the salt-wedge tip. Those are roughly the respective mean annual and minimal summer flow rates when the salt-wedge intrusion is most critical. Similarly as in the previous section for the theoretical analysis in idealized estuaries, we considered SLR values ranging from $\Delta H = 0 \text{ cm}$ (baseline) to $\Delta H = +100 \text{ cm}$ (maximum rise).

Figure 6 shows the computed arrested salt-wedge profiles for case A, defined by $Q = 300 \text{ m}^3/\text{s}$ and a range of SWL that accounts for SLR. Results show how the salt-wedge intrusion length increases with SLR, starting with $L = 11.45 \text{ km}$ for $SWL = +0.0 \text{ m a.s.l.}$, which gradually increases to $L = 19.33 \text{ km}$ for $SWL = +1.0 \text{ m a.s.l.}$ We can notice that the increase of the salt-wedge length is not linear because of variable bottom topography which somewhat governs the intrusion, but the changes in intrusion lengths are evident. Total salt-wedge volumes increase from $V = 42604 \text{ m}^3$ to $V = 77747 \text{ m}^3$. Also, the river inflow needs to increase up to $Q = 375 \text{ m}^3/\text{s}$ to restore the baseline intrusion.

Figure 7 shows the computed arrested salt-wedge profiles for case B, defined by $Q = 50 \text{ m}^3/\text{s}$ and a range of SWL that account for SLR. In contrast to case A, these results show negligible increases in the salt-wedge length. The potential salt-wedge intrusion further upstream is prevented here by a steep channel bed slope. However, an increase in the salt-wedge thickness and volume is evident. Lower layer thickness increases with SLR almost linearly, at Metković station it

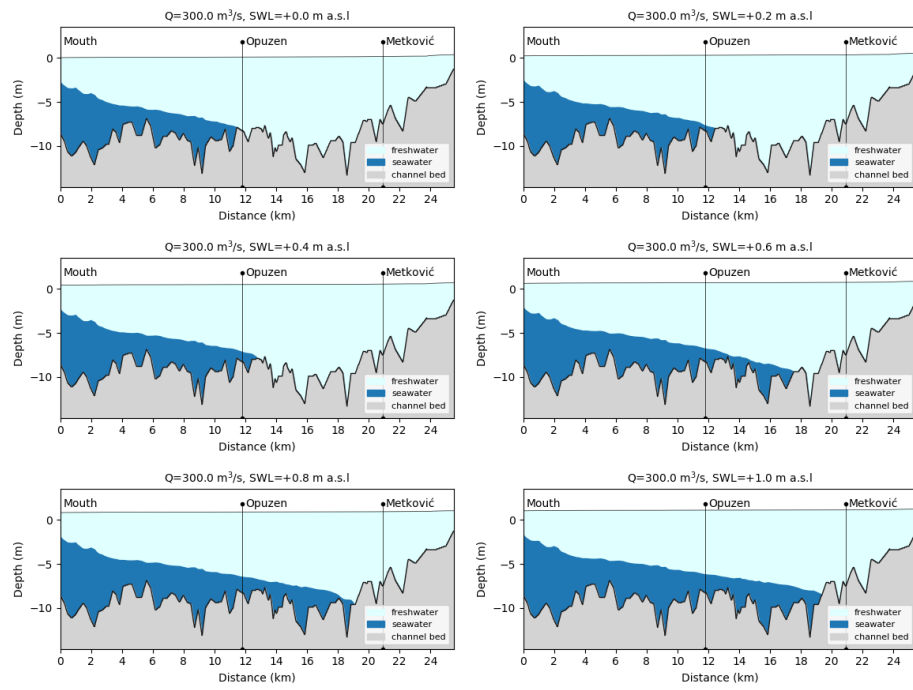


Figure 6: Case A: Longitudinal profiles of computed arrested salt-wedge in the Neretva River Estuary at $Q = 300 \text{ m}^3/\text{s}$ and for SWL ranging from 0 to 100 cm

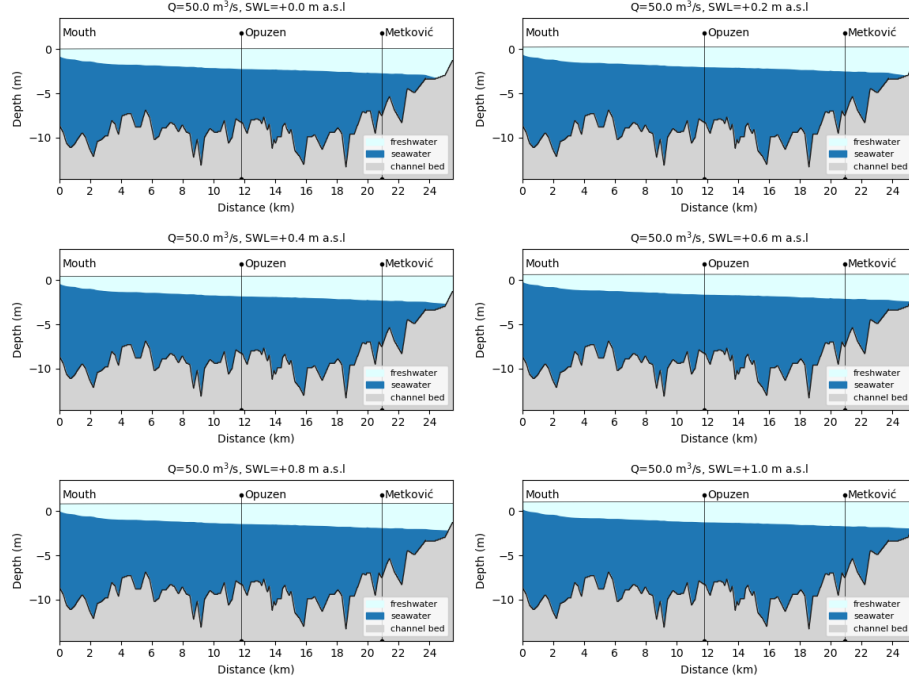


Figure 7: Case B: Longitudinal profiles of computed arrested salt-wedge in the Neretva River Estuary at $Q = 50 \text{ m}^3/\text{s}$ and for SWL ranging from 0 to 100 cm

changes from $h_2 = 4.73 \text{ m}$ for baseline SWL to $h_2 = 5.74 \text{ m}$ for SLR of 1.0 m. Similarly, total salt-wedge volumes increase from $V = 160945 \text{ m}^3$ to $V = 186054 \text{ m}^3$, and the river inflow needs to increase up to $Q = 85 \text{ m}^3/\text{s}$ to restore the baseline intrusion.

Similar behaviour was found in other estuaries. Hong and Shen (2012) also found that the pycnocline depth and seawater volume increases with SLR in the Chesapeake Bay. And Chua and Xu (2014) also considered that an increase of the river inflow needed to maintain intrusion lengths at predefined locations is a good measure of SLR impacts in San Francisco Bay.

5. Discussion

5.1. How suitable is the theoretical approach for the Neretva River Estuary?

In the previous section, we have presented the potential SLR impacts for idealized estuaries using a theoretical approach and for the Neretva River Estuary using a one-dimensional time-dependent numerical model. This section provides a deeper insight into the performance of proposed simple expressions when applied to a realistic microtidal estuary. For this purpose, we computed the relative changes of the salt-wedge length, volume, and corrective river inflow in the Neretva River Estuary and compared them to theoretical values for an idealized 8.5 m deep estuary. This depth corresponds to the mean value of the Neretva River Estuary bottom function downstream from Metkovic station. Note that the results would differ if some other depth was chosen - shorter salt-wedge lengths would be predicted for shallower depths, and vice versa. Fig. 8a-c shows relative changes in the Neretva River Estuary for case A and Fig. 8d-f for case B.

In the first scenario (case A) defined by $Q = 300 \text{ m}^3/\text{s}$ and $F_0 = 0.23$ we notice a very good agreement between theoretical results and the Neretva River Estuary. Relative increases of the salt-wedge length with SLR show some non-linearity, but the overall trend corresponds to theoretical values - for 1.0 m SLR the salt-wedge intrusion length will increase by 69% (Fig. 8a). Similar results are obtained for the salt-wedge volume, which is expected to increase by up to 83% for maximum considered SLR (Fig. 8b). The river inflow increase needed to restore baseline intrusion in the Neretva River Estuary is almost identical to theoretical values and amounts to 25% for maximum considered SLR.

On the other hand, for the second scenario (case B) defined by a lower river inflow $Q = 50 \text{ m}^3/\text{s}$ and $F_0 = 0.16$ we notice significant discrepancies between theoretical values and computed changes in the Neretva River Estuary. Salt-wedge intrusion length seems to be nearly unaffected by SLR (Fig. 8d), although theoretical values in an idealized estuary predict an increase over 60% for 1.0 m SLR. Salt-wedge volumes are increasing with SLR in the Neretva River Estuary

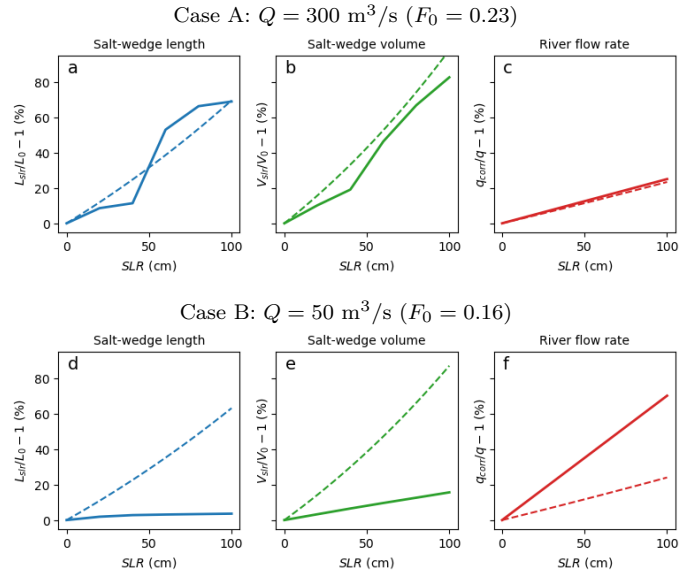


Figure 8: Relative increases of the SLR indicators for cases A and B, where full line (—) denotes modelled results for the Neretva River Estuary and dashed line (---) denotes theoretical results for an idealized 8.5 m deep estuary. First column shows salt-wedge lengths (a, d), second column shows salt-wedge volumes (b, e), and third column shows flow rates needed to restore the baseline intrusion (c, f)

(Fig. 8e), but at a much lower rate than expected for idealized estuaries. On the other hand, corrective river inflows in the Neretva River Estuary are expected to increase by twice as much than for an idealized estuary (Fig. 8f).

The main reason for the discrepancies in the second scenario between theoretical values and numerical results in the Neretva River Estuary is the channel geometry (see Fig. 7). Theoretical salt-wedge intrusion further upstream as predicted in an idealized estuary is prevented by the channel bed in the Neretva River Estuary. Therefore, the salt-wedge length increases only marginally, and the salt-wedge volume primarily reflects a rising pycnocline depth. Higher river inflows are also the results of the steeper bed slope - if the salt-wedge is obstructed by the channel bottom, then much higher river inflow is needed to restore its baseline intrusion length.

The first case suggests that small variations over the mean depth have a minor effect on the salt-wedge intrusion. The second case, on the other hand, indicates that steep channel bed slope has a noticeable impact on the seawater intrusion. This is all in agreement with findings by Poggioli and Horner-Devine (2015), who assessed the sensitivity of salt-wedge estuaries to channel geometry. Yang et al. (2015) also found that the salinity intrusion increases with SLR in the Snohomish River Estuary in the USA are strongly non-linear because of the channel geometry.

5.2. Extending the theoretical solution for sloped estuaries

Considering that the channel geometry seems to significantly affect the potential intrusion of a salt-wedge, and that the theoretical approach derived for idealized flat estuaries cannot capture the impact of geometry, we propose an extension of the original ODE that accounts for a channel bed slope. For this purpose, we rewrite Eq. (7) by introducing a non-uniform channel bed defined by a linear function $b(x) = S_0x$:

$$\frac{dh_1}{dx} = \frac{F_d^2}{1 - F_d^2} C_f \left(1 + r \frac{h_1}{H_0 - S_0x - h_1} \right). \quad (30)$$

where S_0 is the channel bed slope.

We can introduce the same non-dimensional parameters as before (see Eq. (9)) and obtain

$$\frac{d\varphi}{d\chi} = \frac{F_0^2}{\varphi^3 - F_0^2} \left(1 + r \frac{\varphi}{1 - \chi S_0/C_f - \varphi} \right). \quad (31)$$

This ODE, unfortunately, is non-linear for both unknown parameters (φ and χ) and, therefore, it is not possible to find an analytical solution, as was the case for a flat estuary. However, Eqs. (31) or (30) can still be integrated numerically for some channel slope S_0 and interfacial friction factor C_f . Notice that the non-dimensional form of governing ODE introduces a new variable S_0/C_f which can be considered a non-dimensional channel bed slope.

The numerical solutions to Eq. (31) for three different internal Froude numbers are shown in Fig. 9 for horizontal channel bed, as well as a mild and a steep bed slope. The results show that even a mild bed slope can noticeably reduce the potential salt-wedge intrusion length for the same F_0 (Fig. 9b). Figure 9 also indicates that the bed slope impact is more noticeable for lower values of F_0 . Furthermore, notice that when the channel slope becomes steeper, the distinction between salt-wedged for different F_0 is less apparent (Fig. 9c). This confirms our assumption that the potential salt-wedge intrusion with rising sea-level in the Neretva River Estuary is in fact prevented by a channel bed slope (notice the bed elevations from 18 to 25 km in Fig. 1b).

In contrast to flat estuaries, where a salt-wedge may intrude indefinitely upstream when river flow and internal Froude number approach zero, in sloped estuaries, channel bed limits the intrusion. Therefore, the non-dimensional salt-wedge intrusion length function branches into multiple curves depending on the non-dimensional slope S_0/C_f as illustrated in Fig. 10. Equation (31) and Fig. 10 show that as Q and F_0 approach zero, the salt-wedge length approaches a theoretical limit of C_f/S_0 . This is also in agreement with a theoretical analysis of the salt-wedge sensitivity to channel geometry by Poggioli and Horner-Devine (2015).

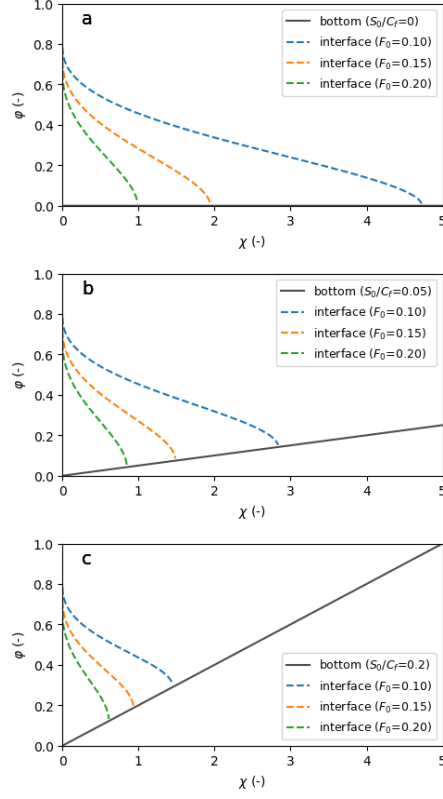


Figure 9: Solution to Eq. (31) - non-dimensional salt-wedge shape - for internal Froude numbers $F_0 = 0.1, 0.15, 0.2$ and for: a) horizontal channel bed (L^* equivalent to Eq. (15)), b) mild channel bed slope $S_0/C_f = 0.05$, c) steep channel bed slope $S_0/C_f = 0.2$

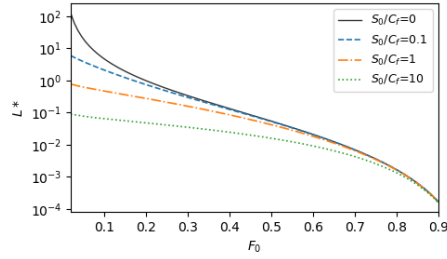


Figure 10: Non-dimensional salt-wedge intrusion length L^* as a function of internal Froude numbers F_0 for different non-dimensional channel bed slopes S_0/C_f

5.3. Advantages and limitations of proposed approaches

Three approaches for assessing SLR impact on salt-wedge intrusion are considered here: a) analytical expressions for idealized estuaries derived from the two-layer theory, b) ODE for sloped estuaries, also derived from the two-layer theory, and c) time-dependant two-layer SWE model for irregular channels derived by extending the two-layer theory. Each of these approaches is increasingly more complex and computationally demanding than the previous one, but with less limitations, and with better accuracy and reliability.

The main limitations of analytical expressions follow from the assumption and simplifications made in deriving them. Temporal effects, such as tidal dynamics, are not accounted for. All contributions from the channel geometry are neglected, including the bed elevations, width variations, as well as transversal and curvilinear effects. Furthermore, the zero thickness pycnocline is rarely found in nature, although in microtidal conditions its thickness may become less than 0.5 m (Ljubenkovic and Vranješ, 2012; Krvavica et al., 2016a). This also means that all vertical processes, including turbulent mixing, are unaccounted for. On the other hand, this method is very simple, easy to use, and it can provide a quick solution for a wide range of parameters.

The ODE approach retains most of these limitations, but it accounts for the channel bed slope. Although it is more accurate and reliable for real estuaries in contrast to analytical expressions, it needs some numerical method to obtain a solution.

In comparison to the two theoretical approaches, the main advantage of STREAM-1D numerical model is that it incorporates temporal effects and a realistic channel geometry. However, the model still has some limitations, such as 2D and 3D effects. This includes transversal and curvilinear channel effects and turbulent processes at the interface, which includes mixing, vertical transport between the layers, and variation of pycnocline thickness. These processes, however, are of secondary importance in microtidal conditions.

6. Conclusion

The impacts of rising sea levels in salt-wedge estuaries are investigated in idealized estuaries using simple expressions derived from a two-layer hydraulic theory and in the Neretva River Estuary in Croatia using a one-dimensional two-layer time-dependent model. The assessment of the SLR impacts was based on three indicators - the salt-wedge intrusion length, the salt-wedge volume, and the river inflows needed to restore the baseline intrusion.

The theoretical analysis in idealized estuaries showed that potential SLR increases all three considered indicators. The results also revealed that shallower estuaries are more sensitive to SLR than deeper estuaries. In comparison to baseline conditions, the salt-wedge intrusion length may increase by more than 150%, the salt-wedge volume by more than 250%, and the river inflows may need to increase by more than 50% to restore the baseline conditions, depending on the estuary depth and the extent of SLR.

The numerical results for the Neretva River Estuary confirmed that potential SLR increases the salt-wedge intrusion. The results, however, indicated that several different indicators should be used when assessing SLR impacts. The salt-wedge intrusion length may be unreliable at low flow conditions due to its high sensitivity to channel geometry. In those case, the salt-wedge volume may be a better indicator because it also reflects the rise of the pycnocline depth with SLR, which may have a negative effect on the salinity intrusion into the aquifer and soil. Corrective river inflow is the most reliable indicator and the most practical one from the viewpoint of water management, but relevant only when some hydraulic structure system is already implemented upstream from the estuary and sufficient water quantities are available for mitigating the salt-wedge intrusion.

In conclusion, the proposed theoretical approach for SLR impacts can be considered a simple and practical tool suitable for preliminary assessment of salinity intrusions in salt-wedge estuaries worldwide. However, theoretical increases of intrusion lengths are meaningful only when predicting changes lower

than maximum possible intrusion lengths, which can be limited by a channel bed slope. A numerical integration of an extended ODE for sloped estuaries is, therefore, a more reliable choice when the channel bed has a pronounced effect, which is usually the case for lower river inflows.

Time-dependant two-layer shallow-water models can accurately capture all relevant consequences of SLR in salt-wedge estuaries and are, therefore, a good alternative to 3D hydrodynamic models. In the Neretva River Estuary, the proposed numerical model was successfully applied to predict impacts from potential SLR and to define appropriate mitigation measures, such as an increase of river inflows needed to restore pre-existing conditions critical for agricultural needs. Overall, the proposed numerical model can be a valuable addition in coastal zone management, especially when assessing the impacts of SLR or any other man-made changes in salt-wedge estuaries.

7. Acknowledgement

Funding: This research was supported by the University of Rijeka, grant number 17.06.2.1.02 Sea and river interaction in the context of climate change and UNIRI-TECHNIC-18-54 "Hydrology of Water Resources and Identification of Risks from Floods and Mud Flows in Karst".

References

- Armi, L., Farmer, D., 1986. Maximal two-layer exchange through a contraction with barotropic net flow. *Journal of Fluid Mechanics* 164, 27–51.
- Bhuiyan, M.J.A.N., Dutta, D., 2012. Assessing impacts of sea level rise on river salinity in the Gorai river network, Bangladesh. *Estuarine, Coastal and Shelf Science* 96, 219–227.
- Bigalbal, A., Rezaie, A., Garzon, J., Ferreira, C., 2018. Potential Impacts of Sea Level Rise and Coarse Scale Marsh Migration on Storm Surge Hydrodynamics and Waves on Coastal Protected Areas in the Chesapeake Bay. *Journal of Marine Science and Engineering* 6, 86.

- Carrasco, A.R., Ferreira, Ó., Roelvink, D., 2016. Coastal lagoons and rising sea level: A review. *Earth-Science Reviews* 154, 356–368.
- Chen, W., Chen, K., Kuang, C., Zhu, D.Z., He, L., Mao, X., Liang, H., Song, H., 2016. Influence of sea level rise on saline water intrusion in the Yangtze River Estuary, China. *Applied Ocean Research* 54, 12–25.
- Chen, W.B., Liu, W.C., Hsu, M.H., 2015. Modeling assessment of a saltwater intrusion and a transport time scale response to sea-level rise in a tidal estuary. *Environmental Fluid Mechanics* 15, 491–514.
- Chua, V.P., Fringer, O.B., 2011. Sensitivity analysis of three-dimensional salinity simulations in North San Francisco Bay using the unstructured-grid SUNTANS model. *Ocean Modelling* 39, 332–350.
- Chua, V.P., Xu, M., 2014. Impacts of sea-level rise on estuarine circulation: An idealized estuary and San Francisco Bay. *Journal of Marine Systems* 139, 58–67.
- Church, J., Clark, P., Cazenave, A., Gregory, J., Jevrejeva, S., Levermann, A., Merrifield, M., Milne, G., Nerem, R., Nunn, P., Payne, A., Pfeffer, W., Stammer, D., Unnikrishnan, A., 2013. *Sea Level Change*. Cambridge University Press, Cambridge, United Kingdom and New York, NY, USA. book section 13. p. 11371216. doi:10.1017/CB09781107415324.026.
- Cui, L., Ge, Z., Yuan, L., Zhang, L., 2015. Vulnerability assessment of the coastal wetlands in the Yangtze Estuary, China to sea-level rise. *Estuarine, Coastal and Shelf Science* 156, 42–51.
- Etemad-Shahidi, A., Rohani, M., Parsa, J., Lemckert, C., 2015. Effects of sea level rise on the salinity of Bahmanshir estuary. *International journal of environmental science and technology* 12, 3329–3340.
- Geyer, W., Ralston, D., 2011. 2.03 The dynamics of strongly stratified estuaries. *Treatise on Estuarine and Coastal Science*. Amsterdam: Elsevier , 37–52.
- Geyer, W.R., MacCready, P., 2014. The estuarine circulation. *Annual review of fluid mechanics* 46, 175–197.

- Geyer, W.R., Scully, M.E., Ralston, D.K., 2008. Quantifying vertical mixing in estuaries. *Environmental fluid mechanics* 8, 495–509.
- Haddout, S., Maslouhi, A., 2018. One-Dimensional hydraulic analysis of the effect of sea level rise on salinity intrusion in the Sebou estuary, Morocco. *Marine Geodesy* 41, 270–288.
- He, W., Zhang, J., Yu, X., Chen, S., Luo, J., 2018. Effect of Runoff Variability and Sea Level on Saltwater Intrusion: A Case Study of Nandu River Estuary, China. *Water Resources Research* 54, 9919–9934.
- Hong, B., Shen, J., 2012. Responses of estuarine salinity and transport processes to potential future sea-level rise in the Chesapeake Bay. *Estuarine, Coastal and Shelf Science* 104, 33–45.
- Ibañez, C., Pont, D., Prat, N., 1997. Characterization of the Ebre and Rhone estuaries: A basis for defining and classifying salt-wedge estuaries. *Limnology and Oceanography* 42, 89–101.
- Jordà, G., Gomis, D., 2013. On the interpretation of the steric and mass components of sea level variability: The case of the mediterranean basin. *Journal of Geophysical Research: Oceans* 118, 953–963.
- Kirwan, M.L., Guntenspergen, G.R., d’Alpaos, A., Morris, J.T., Mudd, S.M., Temmerman, S., 2010. Limits on the adaptability of coastal marshes to rising sea level. *Geophysical research letters* 37.
- Krvavica, N., Kožar, I., Travaš, V., Ožanić, N., 2017. Numerical modelling of two-layer shallow water flow in microtidal salt-wedge estuaries: Finite volume solver and field validation. *Journal of Hydrology and Hydromechanics* 65, 49–59.
- Krvavica, N., Travaš, V., Ožanić, N., 2016a. A field study of interfacial friction and entrainment in a microtidal salt-wedge estuary. *Environmental fluid mechanics* 16, 1223–1246.
- Krvavica, N., Travaš, V., Ožanić, N., 2016b. Salt-Wedge Response to Variable River Flow and Sea-Level Rise in the Microtidal Rječina River Estuary, Croatia. *Journal of Coastal Research* 33, 802–814.

- Krvavica, N., Travaš, V., Ravlić, N., Ožanić, N., 2014. Hydraulics of stratified two-layer flow in Rječina Estuary, in: Proc of 1 st Regional Symposium on Landslides with 3 rd Japanese-Croatian Project Workshop, pp. 257–261.
- Krvavica, N., Tuhtan, M., Jelenić, G., 2018. Analytical implementation of Roe solver for two-layer shallow water equations with accurate treatment for loss of hyperbolicity. *Advances in Water Resources* 122, 187–205.
- Kuang, C., Chen, W., Gu, J., Zhu, D.Z., He, L., Huang, H., 2014. Numerical assessment of the impacts of potential future sea-level rise on hydrodynamics of the Yangtze River Estuary, China. *Journal of Coastal Research* 30, 586–597.
- Li, M., Chen, Z., Finlayson, B., Wei, T., Chen, J., Wu, X., Xu, H., Webber, M., Barnett, J., Wang, M., 2015. Water diversion and sea-level rise: potential threats to freshwater supplies in the Changjiang River estuary. *Estuarine, Coastal and Shelf Science* 156, 52–60.
- Ljubenkovic, I., 2015. Hydrodynamic modeling of stratified estuary: case study of the Jadro River (Croatia). *Journal of Hydrology and Hydromechanics* 63, 29–37. doi:10.1515/johh-2015-0001.
- Ljubenkovic, I., Vranješ, M., 2012. Numerical model of stratified flow- case study of the Neretva riverbed salination(2004). *Gradevinar* 64, 101–112.
- van Maanen, B., Sottolichio, A., 2018. Hydro-and sediment dynamics in the Gironde estuary (France): sensitivity to seasonal variations in river inflow and sea level rise. *Continental Shelf Research* 165, 37–50.
- MacDonald, D.G., Geyer, W.R., 2004. Turbulent energy production and entrainment at a highly stratified estuarine front. *Journal of Geophysical Research: Oceans* 109.
- Mahgoub, M., Hinkelmann, R., La Rocca, M., 2014. Understanding the behaviour of gravity currents in tideless estuaries and considering the impact of sea level rise within the Nile Estuary. *Journal of Coastal Research* 31, 714–722.
- Mohammed, R., Scholz, M., 2017. Critical review of salinity intrusion in rivers and estuaries. *Journal of Water and Climate Change* 9, 1–16.

- Monismith, S.G., Kimmerer, W., Burau, J.R., Stacey, M.T., 2002. Structure and flow-induced variability of the subtidal salinity field in northern San Francisco Bay. *Journal of Physical Oceanography* 32, 3003–3019.
- Oskoruš, D., Krvavica, N., Švonja, M., 2019. Method for calculating daily discharges of the Neretva River at Metković, in: 7. Croatian Water Conference (In Croatian).
- Poggioli, A.R., Horner-Devine, A.R., 2015. The sensitivity of salt wedge estuaries to channel geometry. *Journal of Physical Oceanography* 45, 3169–3183.
- Prandle, D., Lane, A., 2015. Sensitivity of estuaries to sea level rise: Vulnerability indices. *Estuarine, Coastal and Shelf Science* 160, 60–68.
- Ralston, D.K., Geyer, W.R., Lerczak, J.A., Scully, M., 2010. Turbulent mixing in a strongly forced salt wedge estuary. *Journal of Geophysical Research: Oceans* 115.
- Rezo, M., Pavasović, M., 2014. Analiza mareografskih podataka o Jadranskom moru od 1953 . do 2006 . godine. *Geodetski list* 4, 269–290. (In Croatian).
- Rice, K.C., Hong, B., Shen, J., 2012. Assessment of salinity intrusion in the James and Chickahominy Rivers as a result of simulated sea-level rise in Chesapeake Bay, East Coast, USA. *Journal of Environmental Management* 111, 61–69.
- Ross, A.C., Najjar, R.G., Li, M., Mann, M.E., Ford, S.E., Katz, B., 2015. Sea-level rise and other influences on decadal-scale salinity variability in a coastal plain estuary. *Estuarine, Coastal and Shelf Science* 157, 79–92.
- Sampath, D.M.R., Boski, T., 2016. Morphological response of the saltmarsh habitats of the Guadiana estuary due to flow regulation and sea-level rise. *Estuarine, Coastal and Shelf Science* 183, 314–326.
- Sargent, F.E., Jirka, G.H., 1987. Experiments on saline wedge. *Journal of hydraulic engineering* 113, 1307–1323.
- Schijf, J., Schönfeld, J., 1953. Theoretical considerations on the motion of salt and fresh water, in: *Proceedings Minnesota International Hydraulic Convention, IAHR*.
- Shaha, D.C., Cho, Y.K., Kim, T.W., 2012. Effects of river discharge and tide driven sea level variation on saltwater intrusion in Sumjin River estuary: an application of finite-volume coastal ocean model. *Journal of Coastal Research* 29, 460–470.

- Shalem, Y., Yechieli, Y., Herut, B., Weinstein, Y., 2019. Aquifer response to estuarine stream dynamics. *Water* 11, 1678.
- Stommel, H., Farmer, H.G., 1953. Control of salinity in an estuary by a transition. *J. Mar. Res* 12, 13–20.
- Tian, R., 2019. Factors controlling saltwater intrusion across multi-time scales in estuaries, chester river, chesapeake bay. *Estuarine, Coastal and Shelf Science* 223, 61–73.
- Tritton, D., 1988. *Physical fluid dynamics*. Second ed., Oxford University Press.
- Tsimplis, M.N., Raicich, F., Fenoglio-Marc, L., Shaw, A.G., Marcos, M., Somot, S., Bergamasco, A., 2012. Recent developments in understanding sea level rise at the Adriatic coasts. *Physics and Chemistry of the Earth, Parts A/B/C* 40, 59–71.
- Tsz Yeung Leung, A., Stronach, J., Matthieu, J., 2018. Modelling Behaviour of the Salt Wedge in the Fraser River and Its Relationship with Climate and Man-Made Changes. *Journal of Marine Science and Engineering* 6, 130.
- Vilibić, I., Šepić, J., Pasarić, M., Orlić, M., 2017. The Adriatic Sea: a long-standing laboratory for sea level studies. *Pure and Applied Geophysics* 174, 3765–3811.
- Yang, Z., Wang, T., Voisin, N., Copping, A., 2015. Estuarine response to river flow and sea-level rise under future climate change and human development. *Estuarine, Coastal and Shelf Science* 156, 19–30.